



HAL
open science

The Indonesian Throughflow response to Indo-Pacific climate variability

Janet Sprintall, Adèle Révelard

► **To cite this version:**

Janet Sprintall, Adèle Révelard. The Indonesian Throughflow response to Indo-Pacific climate variability. *Journal of Geophysical Research. Oceans*, 2014, 119 (2), pp.1161 - 1175. 10.1002/2013jc009533 . hal-01496468

HAL Id: hal-01496468

<https://hal.science/hal-01496468>

Submitted on 3 Jan 2022

HAL is a multi-disciplinary open access archive for the deposit and dissemination of scientific research documents, whether they are published or not. The documents may come from teaching and research institutions in France or abroad, or from public or private research centers.

L'archive ouverte pluridisciplinaire **HAL**, est destinée au dépôt et à la diffusion de documents scientifiques de niveau recherche, publiés ou non, émanant des établissements d'enseignement et de recherche français ou étrangers, des laboratoires publics ou privés.

Copyright

RESEARCH ARTICLE

10.1002/2013JC009533

Special Section:

Western Pacific Ocean
Circulation and Climate

The Indonesian Throughflow response to Indo-Pacific climate variability

Janet Sprintall¹ and Adèle Révelard²¹Scripps Institution of Oceanography, U.C. San Diego, La Jolla, California, USA, ²LOCEAN/IPSL, Université Pierre et Marie Curie, Paris, France

Key Points:

- A proxy 18 year Indonesian Throughflow (ITF) transport time series is developed
- Increased ITF transport related to enhanced Pacific tradewinds since early 1990s
- Indian Ocean dynamics dominate Pacific ENSO variability in ITF outflow passages

Correspondence to:

J. Sprintall,
jsprintall@ucsd.edu

Citation:

Sprintall, J., and A. Révelard (2014), The Indonesian throughflow response to Indo-Pacific climate variability, *J. Geophys. Res. Oceans*, 119, 1161–1175, doi:10.1002/2013JC009533.

Received 21 OCT 2013

Accepted 10 JAN 2014

Accepted article online 15 JAN 2014

Published online 19 FEB 2014

Abstract The Indonesian Throughflow (ITF) is the only open pathway for interocean exchange between the Pacific and Indian Ocean basins at tropical latitudes. A proxy time series of ITF transport variability is developed using remotely sensed altimeter data. The focus is on the three outflow passages of Lombok, Ombai, and Timor that collectively transport the entire ITF into the Indian Ocean, and where direct velocity measurements are available to help ground-truth the transport algorithm. The resulting 18 year proxy time series shows strong interannual ITF variability. Significant trends of increased transport are found in the upper layer of Lombok Strait, and over the full depth in Timor Passage that are likely related to enhanced Pacific trade winds since the early 1990s. The partitioning of the total ITF transport through each of the major outflow passage varies according to the phase of the Indian Ocean Dipole (IOD) or El Niño-Southern Oscillation (ENSO). In general, Pacific ENSO variability is strongest in Timor Passage, most likely through the influence of planetary waves transmitted from the Pacific along the Northwest Australian shelf pathway. Somewhat surprisingly, concurrent El Niño and positive IOD episodes consistently show contradictory results from those composites constructed for purely El Niño episodes. This is particularly evident in Lombok and Ombai Straits, but also at depth in Timor Passage. This suggests that Indian Ocean dynamics likely win out over Pacific Ocean dynamics in gating the transport through the outflow passages during concurrent ENSO and IOD events.

1. Introduction

The Indonesian Throughflow (ITF) is the leakage of water from the western Pacific into the south-eastern tropical Indian Ocean through the Indonesian archipelago (Figure 1). As such, the ITF provides the only major low-latitude oceanic pathway for the transfer of climate signals and their anomalies in the global thermohaline circulation. The volume, heat, and freshwater carried by the ITF are known to impact the state of the Pacific and Indian Oceans, and modulate regional climate variability through altering the regional air-sea exchange and precipitation patterns over many time scales [e.g., Nicholls, 1989; Godfrey, 1996; Schneider, 1998; Lee *et al.*, 2002; Vranes *et al.*, 2002; Potemra and Schneider, 2007; Song *et al.*, 2007; Lee and McPhaden, 2008; Tokinaga *et al.*, 2012]. In turn, winds over the Pacific and Indian Oceans as well as the regional Indonesian seas impact the ITF through the excitation and propagation of planetary waves [Clarke and Liu, 1994; Meyers, 1996; Sprintall *et al.*, 2000; Potemra, 2001; Wijffels and Meyers, 2004; McClean *et al.*, 2005].

On annual and longer time scales, the ITF is driven by the large-scale pressure difference that exists between the Pacific and Indian Ocean basins [Wyrski, 1987]. The pressure gradient is set up because, on average, the Pacific easterly trade-winds result in a higher sea level on the western tropical Pacific side of the Indonesian archipelago compared to the monsoonally regulated sea level in the ITF exit region of the south-eastern Indian Ocean. Most models and observations suggest a weaker ITF during El Niño in response to the Pacific trade-wind relaxations or reversals that subsequently lead to a lower western Pacific sea level [Clarke and Liu, 1994; Meyers, 1996; Gordon *et al.*, 1999]. The opposite conditions are expected to prevail during La Niña. Pacific Ocean interannual wind anomalies potentially force low-frequency equatorial and off-equatorial Rossby waves that interact with the western Pacific maritime boundary to excite a coastally trapped response that propagates through the Indonesian seas, along the northwest coast of Australia, and then offshore into the Indian Ocean [Wijffels and Meyers, 2004; McClean *et al.*, 2005; England and Huang, 2005]. Like ENSO, the Indian Ocean Dipole (IOD) appears to influence the ITF transport via remotely forced Kelvin waves related to the equatorial Indian Ocean wind anomalies [Sprintall *et al.*, 2009; Drushka *et al.*,

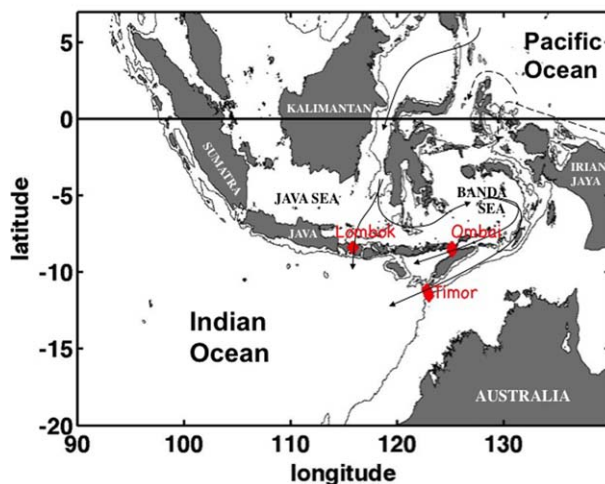


Figure 1. Map of the Indonesian seas showing pathways of the Indonesian Throughflow from the Pacific Ocean into the Indian Ocean. Lombok, Ombai, and Timor Straits are the major outflow passages of the ITF where moorings were located as part of INSTANT (red diamonds).

2010]. However, because of the frequent concurrence of ENSO and IOD events [Murtugudde et al., 1998; Saji et al., 1999; Feng et al., 2001; Potemra and Schneider, 2007], it is often difficult to tease out the individual effect of each climate mode on the ITF variability.

The recent 3 year International Nusantara Stratification and Transport (INSTANT) program provided the first simultaneous full-depth velocity and transport measurements in the major inflow and outflow passages of the ITF [Sprintall et al., 2004; Gordon et al., 2010]. The INSTANT time period was characterized by a weak warm phase of ENSO (El Niño) from the initial deployment in January 2004 until October 2005, followed by a brief cool phase (La Niña) until April 2006, with stronger El Niño conditions occurring until the mooring recovery in December 2006. The developing El Niño conditions in the Pacific during this latter period also coincided with a strong IOD positive phase in the Indian Ocean that terminated in December 2006 to January 2007 [Vinayachandran et al., 2007; Horii et al., 2008]. While the 3 year time series alone is not sufficient to comprehensively resolve the interannual signal, significant transport variability during the INSTANT period was linked to ENSO and the IOD [Sprintall et al., 2009; Gordon et al., 2008]. The strong positive phase of the IOD in late 2006 appeared to decrease the ITF transport through the outflow passages at depth, but the transport in the upper 150 m layer was stronger, hence somewhat negating the expected weakening associated with the concurrent 2006 El Niño [Sprintall et al., 2009]. In contrast, during the 2004 El Niño when the IOD was near zero, the ITF transport was reduced in the upper 150 m surface layer but enhanced at depth. Clearly, the relatively short 3 year record makes it difficult to separate the competing remote influences from the IOD and ENSO and thus provide an adequate description of how these low-frequency fluctuations impact the ITF transport. Observational programs such as INSTANT can be logistically difficult and expensive to maintain over time scales long enough to be important to climate variability. The challenge is to develop a proxy measurement of the ITF transport that adequately captures the dominant time scales of throughflow dynamics, and in turn, improves our ability to understand its relationship to longer-term climate variability.

Thus, while recent observational and modeling studies have furthered our knowledge of the interannual variability of the ITF, many questions remain unanswered that provide the fundamental drivers of this study. How does the partitioning of the total ITF transport through the major ITF passages vary according to the phase of the IOD or ENSO? Are the changes in transport in response to local or large-scale remote wind forcing? To address these issues, we will develop ITF proxy measurements using the 18 year remotely sensed altimetry record. Our focus is on the three outflow passages of Lombok, Ombai, and Timor, where the direct INSTANT 3 year transport measurements are available to help mold and ground-truth the algorithm needed to convert the sea level data to ITF transport information. Together, these three outflow straits comprise the total ITF transport that enters into the southeast Indian Ocean. However, the gating of the total ITF transport through each major outflow passage potentially varies according to the phase of the IOD and/or ENSO, although this has yet to be thoroughly constrained by observations. Each strait transports waters with different temperature and salinity characteristics [Sprintall et al., 2009; Atmadipoera et al., 2009], and consequently each strait will have a different impact on the heat and freshwater transports that enters into Indian Ocean.

This paper is organized as follows. Section 2 discusses the data sets used in this study, and section 3 describes the partial-linear regression technique used to develop the 18 year proxy time series. Section 4 evaluates variability and long-term trends in the transport time series, and also examines how the

Table 1. Classification of Years When El Niño or La Niña Events Coincided With a Positive or Negative Indian Ocean Dipole (IOD) Event From 1993 Through 2010

	Negative IOD	No IOD event	Positive IOD
El Niño		2002, 2004, 2009	1994, 1997, 2006
No ENSO event	1996	1993, 2001, 2003, 2008	
La Niña	1998, 2010	1995, 1999, 2000, 2005	2007

partitioning of the total ITF transport through each major outflow passage varies according to the phase of the IOD or ENSO. A discussion follows in section 5 to assess how these changes vary in response to local and large-scale remote wind forcing. Conclusions follow in Section 6.

2. Data

The in situ transport data used in this study were measured as part of the INSTANT program (Figure 1). During the 3 year INSTANT deployment period from January 2004 through December 2006, two moorings were deployed in Lombok Strait (sill depth ~300 m), two moorings were deployed in Ombai Strait (sill depth ~3250 m), and four moorings were deployed in the wider Timor Passage (western sill depth ~1890 m). Mooring velocity instrumentation was fairly similar on all moorings, with an upward-looking acoustic Doppler current profiler (ADCP) deployed to resolve the surface to lower-thermocline flow and discrete current meters at depth. To estimate the total volume transport through each of these major outflow straits, the velocity profiles were vertically linearly interpolated onto a 10 m depth grid, then laterally interpolated into 1 km bins between the moorings and extrapolated to the strait side-walls using various models (see *Sprintall et al.*, [2009], for more details). In the following analysis, the daily transport values correspond to the “best” interpolation scheme [*Sprintall et al.*, 2009] that use a constant shear model for the missing near-surface layer and a linear cross-passage interpolation scheme. As noted above, in all three passages a clear phase break was observed at 150 m depth where the transport anomalies above and below this depth exhibited opposing directions on interannual time scales [*Sprintall et al.*, 2009]. Vertical decomposition of transport profiles in the outflow passages into two modes has previously been suggested using both models [*Potemra et al.*, 2003] and observations [*Molcard et al.*, 2001]. Hence, in the following, separate proxies will be developed for transport integrated over the upper layer (0–150 m) and lower layer (150 m to sill depth). The sign-convention is that transport into the Indian Ocean (i.e., the ITF) is negative.

The sea level anomaly (SLA) data used here to develop proxy measurements of the ITF comes from gridded delayed-time maps distributed by Aviso. The version utilized is the reference version (DT-MSLA-“ref”), in which data sets are based on at least two satellites with the same groundtrack. The daily data are available from October 1992 to January 2011 and have a resolution of 1/3° longitude by 1/3° latitude.

The ocean surface wind and pseudostress is provided by NASA’s Cross-Calibrated Multi-Platform (CCMP) project that includes cross-calibrated satellite winds derived from a combination of many radar scatterometers [*Atlas et al.*, 2011]. We use the CCMP FLK Level 3.5 wind product that has a resolution of 1/4° longitude by 1/4° latitude and are monthly.

To examine the relationship of our proxy ITF time series to large-scale climate modes, we use the weekly ENSO and IOD indices based on sea surface temperature (SST) anomalies. A positive SST anomaly corresponds to a warm El Niño phase and a negative anomaly to a cold La Niña phase. Typically, an El Niño event begins in boreal spring and peaks in the following fall/winter, although there are occasional exceptions to this generality (e.g., 1994). To evaluate the corresponding ENSO phase of each month, we use the recent Oceanic Niño Index (ONI) from the NOAA Climate Prediction Center that is based on the detrended NINO3.4 SST anomalies centered on 30 year base periods that are updated every 5 years so as to account for longer-term secular trends. For the IOD, we use the index time series based on the difference in SST anomaly between the tropical western and the tropical south-eastern Indian Ocean [*Saji et al.*, 1999] provided by the Japan Agency for Marine-Earth Sciences and Technology (JAMSTEC). A positive IOD event/index corresponds to when the SST is anomalously cold in the eastern Indian Ocean and anomalously warm in the western Indian Ocean. The reverse occurs during negative events. IOD episodes are much more phase locked to the seasonal cycle than ENSO episodes, and typically begin during the monsoon boreal spring transition and peak during the boreal fall. Table 1 lists those years that correspond to negative and positive phases of both the IOD and ENSO.

3. Methodology

The idea that ITF transport could be estimated from sea-level differences between the Pacific and Indian Oceans was first proposed by Wyrcki [1987], who suggested that the large-scale pressure difference between the two basins provided the forcing of the ITF on annual and longer time scales. The concept was initially explored in the Indonesian region using sea level differences and patterns from tide gauges [Wyrcki, 1987; Clarke and Liu, 1994]. The advent of the global satellite era provoked further exploration of the relationship between the altimetric sea level record with the ITF transport determined using both numerical model output [Potemra et al., 1997; Potemra, 2005], and temperature profiles measured along three expendable bathythermograph (XBT) transects within the Indonesian seas [Wijffels and Meyers, 2004]. Such an approach has also been used or proposed for various moored time series arrays [e.g., Imawaki et al., 2001; van Sebille et al., 2010; Ferrari et al., 2012]. The strategy of these particular studies was to align their in situ moored arrays with a collocated altimetric track and develop a transport-local sea level relationship to subsequently extend the observed time series.

In this study, proxy transports are developed using the regional SLA regressed onto the in situ measured ITF transport within the three major outflow passages of Lombok Strait, Ombai Strait, and Timor Passage [Sprintall et al., 2009]. The obvious advantage in the proposed analysis over the previous proxy ITF studies is that actual observed ITF transport measurements within the passages are available. Further, in our study we exploit the premise that it is primarily the large-scale Indo-Pacific pressure gradient that drives the ITF on interannual time scales [Wyrcki, 1987]. Hence, we develop the relationship using the regional SLA fields rather than use the locally aligned SLA, which also alleviates the issues of accuracy in the altimetric sampling near the coast in these relatively narrow passages.

3.1. Technique for Development of Proxy Transports

Strong correlations exist between the regional SLA and the INSTANT transport time series in each outflow passage over the upper 150 m depth layer (Figures 2a–2c) and the layer beneath this (Figures 2d–2e). In the upper layer, Lombok (Figure 2a) and Ombai (Figure 2b) Straits show very similar correlation patterns, with highly significant positive correlations in the south-east Indian Ocean along the wave guide of the south coasts of Sumatra and Java, as well as in the western Pacific region. Positive correlations are of the sense that an increase in SLA is associated with reduced transport into the Indian Ocean (recall that the ITF transport is negative). In contrast, the upper layer in Timor Passage has little correlation with the south-east Indian Ocean wave guide, and is mostly negatively correlated with the SLA in the western Pacific and internal Indonesian seas, suggesting a stronger ITF corresponds to higher sea level (Figure 2c). This relationship holds in the western Pacific for the lower layer of Timor Passage (Figure 2e), while in the Indian Ocean the positive correlation suggests a reduced ITF with higher sea level, as in the lower layer of Ombai Strait (Figure 2d).

Similar to that found by Potemra [2005], the highest transport-SLA correlations (Figure 2) generally occur in regions of known dynamical influence on ITF variability through remote and local wind forcing. As succinctly put by Wijffels and Meyers [2004], this likely reflects the fact that the Indonesian seas lie at an “intersection of oceanic waveguides” from the Pacific and Indian Oceans. Six regions are identified that consistently showed the strongest transport-SLA correlations (Figure 2). We exploit this tight relationship through the linear, lagged partial regression model,

$$Q'_{ITF(t)} = \sum_i \sum_j \alpha_{ij} \eta_i(t - \delta t_j) \tag{1}$$

to develop a proxy-ITF transport time series Q'_{ITF} that at time t is expressed as a sum of the average sea level anomaly in each box η_i at time lag δt_j with coefficients α_{ij} representing the respective weight of the i th SLA box at the j th time lag. All transport and sea level time series were demeaned and normalized to have unit variance before performing the least squares fit, so the coefficients represent the transport change associated with a one-unit standard deviation change in the sea level time series. The coefficients and lags were determined from a least squares fit of the 3 year upper (0–150 m) and lower (150 m—sill depth) layer INSTANT transport in each of the three passages with, in the first instance, the sea level in all six boxes. A broad range of time lags was applied covering from 140 days which is roughly equivalent to the time Pacific

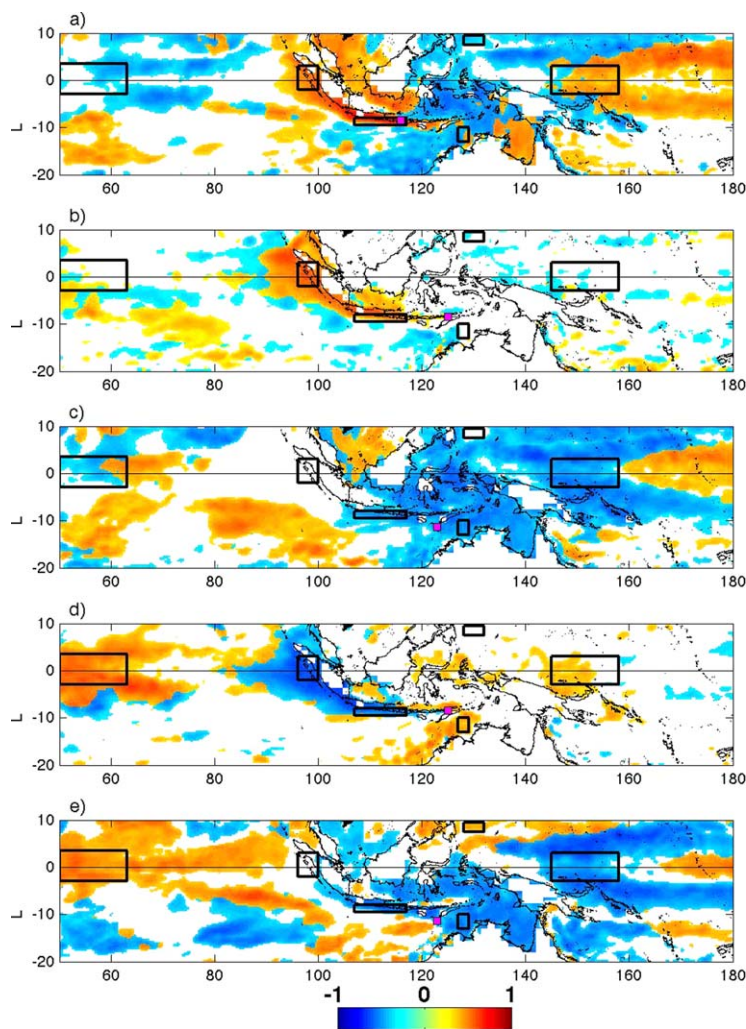


Figure 2. (a) Maximum correlation between SLA and INSTANT transport through (a) Lombok, (b) Ombai, and (c) Timor over the 0–150 m depth layer; and transport through (d) Ombai and (e) Timor from 150 m to the sill depth. Moorings in each strait are marked by a magenta square. Boxes show regional SLA used in forming the proxy transports.

the derived regression coefficients. In the end, this resulted in each transport time series through the three passages typically represented by three to four terms in equation (1) that represented the lags and regional boxes that had the strongest correlations. As discussed below, in nearly all cases these optimal lags and regional boxes also made sense from a dynamical point of view.

The resulting best fit linear prediction model given by equation (1) does a good job of capturing the low-frequency variability and shows significant correlations of ~ 0.8 with the respective observed time series in each strait (Figure 3). The best agreement occurs in the shallower Lombok Strait where the total amount of variance accounted for by the lagged partial regression model is $\sim 80\%$ (Figure 3a). Here sea level in the region south of Java at zero lag ($\alpha_{SJ,0} = 1.26$) and in the equatorial Indian Ocean at 120 day lags ($\alpha_{IND,120} = -0.75$) influence the transport variability in the shallow Lombok Strait emphasizing the importance of Indian Ocean processes. In Ombai Strait, the lagged model accounts for $\sim 70\%$ of the total variance in both the upper (Figure 3b) and lower layer (Figure 3d) transport. As in Lombok Strait, sea level south of Java has the strongest correlation with transport variability in the upper ($\alpha_{SJ,7} = 0.88$) and lower ($\alpha_{SJ,14} = 1.66$) layers, with the lags consistent with the phasing of the passage of Kelvin waves from south of Java into Ombai Strait. Somewhat surprisingly, the deeper layer in Ombai Strait is also influenced by sea level variability near Darwin at 21 day lag ($\alpha_{DAR,21} = -0.66$), and has a relatively quick response to sea level variability 14 days earlier in the western Pacific ($\alpha_{WP,14} = 0.74$). Consistent with the Pacific Ocean wave guide

sea level signals take to reach the eastern Indian Ocean [Masumoto and Meyers, 1998; Wijffels and Meyers, 2004] to 0 days (i.e., immediate local response). Note that by including all possible sea level boxes and time lags, we are able to reproduce the observed INSTANT transport series nearly perfectly. However, then the prediction becomes too tuned to the variability captured at the same frequencies as occur in the observed training data set, and so become unreliable for developing longer-term proxies for studies of low-frequency variability. In our methodology, the skill of the contributed fit from each sea level box and lag combination was assessed through standard t tests that determine significance of each coefficient followed by application of bootstrapping techniques [Efron and Gong, 1983] that reduce the size of the training data set to test sensitivity of

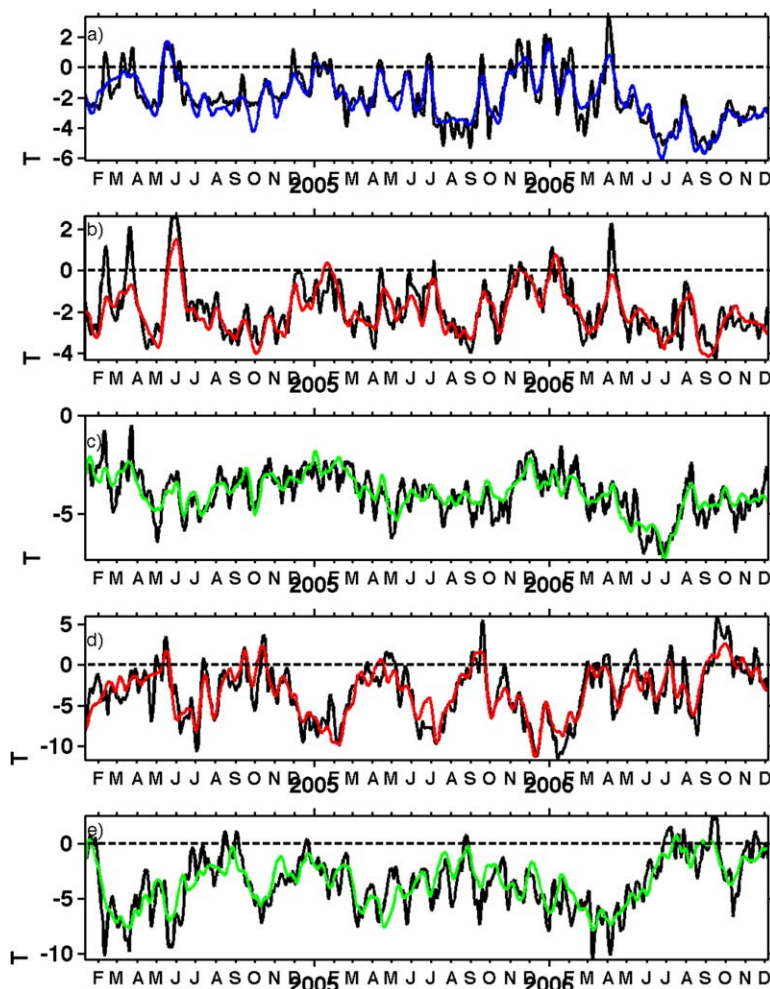


Figure 3. Time series of observed (black) and predicted (color) transports (Sv) in (a) Lombok, (b) Ombai, and (c) Timor over the depth range 0–150 m; and (d) Ombai and (e) Timor over the depth range from 150 m to sill depth during the INSTANT program (2004–2006).

influence along the north-west Australian shelf [Wijffels and Meyers, 2004], in Timor Passage the sea level variability near Darwin influences the upper layer transport (Figure 3c) on relatively short time lags of 7 days ($\alpha_{\text{DAR},7} = -0.85$) and the lower layer (Figure 3e) on longer time scales ($\alpha_{\text{DAR},120} = -1.17$), while the western Pacific sea level variability influences the deep Timor transport over a range of time lags ($\alpha_{\text{WP},0} = -0.92$ to $\alpha_{\text{WP},120} = -0.5$). Including the sea level variations from the Indian Ocean and south of Java only marginally improved the skill of the prediction in Timor's lower layer, but made a significant contribution to the upper layer ($\alpha_{\text{SJ},7} = 0.93$). Although included in Wyrtki's [1987] original analysis, sea level variability at Davao had negligible influence on transport through all the outflow passages.

The derived coefficients from the multiregression models (1) are then

applied to the SLA from the identified binned regions at the optimized lags to extend the proxy time series to the length of the altimeter mission record (i.e., from ~January 1993 through January 2011).

3.2. Comparison of the Proxy Transport With Independent Observations

There exist relatively few in situ measurement time series in the outflow passages other than the INSTANT program with which to independently validate our proxy transports. Over the time span of the proxy transports, only Ombai Strait [Molcard *et al.*, 2001] provides some data for comparison, although as discussed below, there are some issues that complicate direct comparison with the derived proxy time series.

Ombai Strait transport was measured by a mooring deployed from December 1995 through November 1996 [Molcard *et al.*, 2001]. The single mooring was deployed at the same location as the Ombai South mooring deployed during INSTANT, and as such should capture the main core of the ITF that lies in the southern part of Ombai Strait [Sprintall *et al.*, 2009]. However, the reversals associated with the eastward flowing South Java Current and Undercurrent system that hug the northern walls of Ombai Strait that were captured by the Ombai North mooring during INSTANT [Sprintall *et al.*, 2010] would be missed by the single mooring in 1996. In addition, the vertical resolution of the velocity-measuring instruments distributed along the mooring line in 1996 was not as dense as during INSTANT, in particular during 1996 only two current meters were located below 150 m at 1020 m and 1220 m (compare Figure 3 in Molcard *et al.* [2001] with Figure 3 in Sprintall *et al.* [2009]). The transport from the 1996 Ombai mooring velocity data was estimated

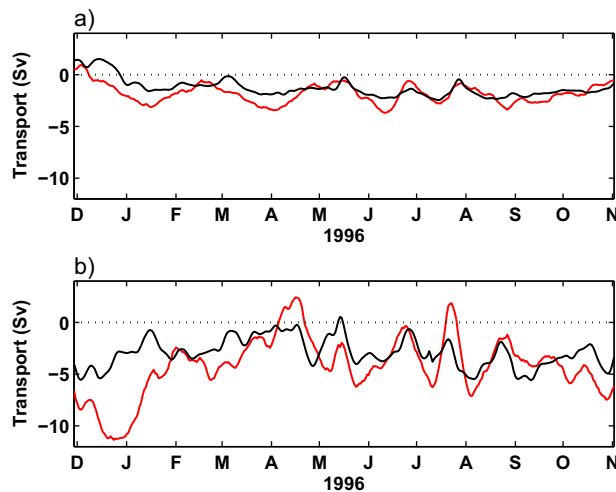


Figure 4. (a) Upper layer (0–150 m) and (b) lower layer (150 m—sill depth) predicted proxy (red) and observed (black) transport in Ombai Strait in 1996.

and -1.3 ± 0.9 Sv observed transport for the upper layer, and -4.2 ± 2.8 Sv proxy transport and -2.9 ± 1.4 Sv observed transport for the lower layer. The poorer agreement with the lower layer largely stems from the beginning of the record, when the predicted proxy transport is nearly twice that of the observed transport in December 1995 (Figure 4b). This period coincides with the arrival of a Kelvin wave in Ombai Strait [Molcard *et al.*, 2001] and the transport reversal associated with the wave is evident in both the observed and predicted transport in the upper layer (Figure 4a). The significantly larger predicted transport in the lower layer is consistent with that observed in Ombai Strait during INSTANT, when during Kelvin wave events the main core of the westward flowing ITF extends from ~ 150 m to 600 m [Sprintall *et al.*, 2009]. It is likely that the vertical instrument configuration during the 1996 observation period missed this contribution from the deeper ITF and so somewhat underestimates the lower layer transport (Figure 4b).

4. Transport Variability

Our goal is to use the resultant 18 year ITF proxy time series to investigate the dominant time scales of throughflow dynamics and improve our understanding of the response of the ITF to interannual climate modes such as ENSO and IOD. In this section, we first compare the seasonal cycle based on the annual and semiannual harmonics from this 18 year proxy time series with the 3 year INSTANT time series. Our focus is then on the longer term variability, and we form “interannual” anomalies by removing the seasonal cycle and low pass (180 days) filtering the proxy time series. The resultant time series is used to examine long-term trends, as well as an attempt to tease out how the partitioning of the total ITF transport through each of the major outflow passage varies according to the phase of the IOD or ENSO.

4.1. The Seasonal Cycle

The circulation and transport within the Indonesian seas has a large seasonal variation due to the influence of the reversing annual wind patterns associated with the Asian-Australian monsoon system [Clarke and Liu, 1993; Masumoto and Yamagata, 1996; Sprintall *et al.*, 2009]. Relatively dry winds blow from the southeast across the region during the Southeast Monsoon (SEM) of June–August, while moist warm air blows from the west during the Northwest Monsoon (NWM). Between these times, the monsoon transition is marked by westerly wind bursts as the intertropical convergence zone crosses the equator in both the Pacific and the Indian Oceans.

In the upper 150 m, there is generally good agreement between phases of the seasonal cycle from the 3 year INSTANT time series and that from the predicted 18 year proxy time series (Figure 5). It is important to note that there is no reason to expect perfect agreement, since the two time series differ in length and cover different phases of the ENSO and IOD cycles that likely modulate the phenology of the seasonal transport. Maximum transport in the upper layer occurs during the peak of the SEM in Timor Passage, and at the end of the

using the same vertical and cross-passage interpolation scheme as applied to the INSTANT time series used to form the proxy (see section 2), and integrated over the upper 150 m (Figure 4a) and from 150 m to sill depth (Figure 4b).

Despite the apparent shortcomings of the comparison, the 1996 Ombai transport and the concurrent predicted proxy transport time series show very similar patterns, with significant correlations of 0.68 in the upper layer and 0.51 in the lower layer. The mean and standard deviations over the complete time period are -1.8 ± 0.9 Sv proxy transport

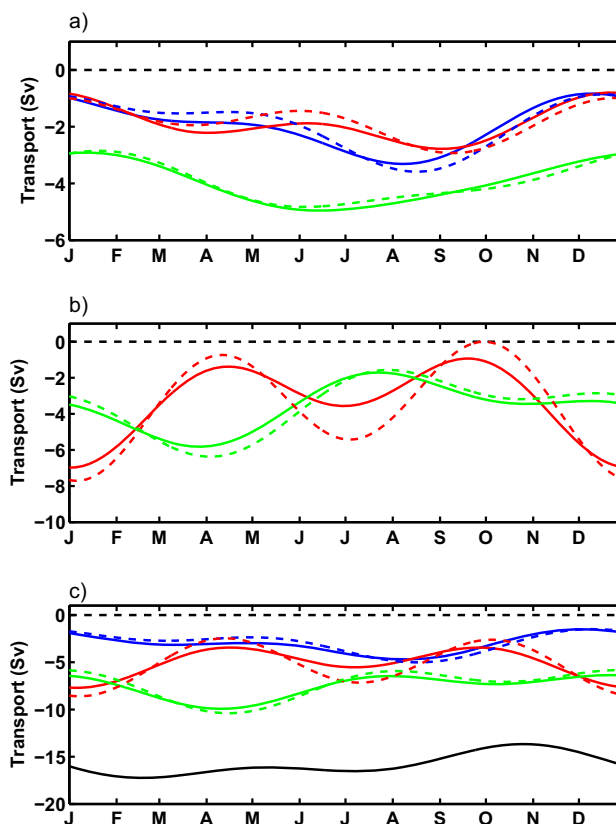


Figure 5. Seasonal time series of predicted (solid) and observed (dashed) transports in Lombok Strait (blue), Ombai Strait (red), and Timor Passage (green) over the depth range (a) 0–150 m; (b) 150 m to sill depth; and (c) full depth. Seasonal transports are estimated from harmonics with both a semiannual and annual component. Total full depth transport summed over all three passages is shown in black in Figure 5c.

4.2. Interannual Variability and Long-Term Trends

Anomalous interannual proxy transport time series were produced by removing the seasonal cycle from the original time series then low-pass filtering with a 180 day Hamming filter (Figure 6). As noted, the 3 year INSTANT period (2004 through 2006) was characterized by remarkably similar interannual transport anomalies in all three outflow passages [Sprintall *et al.*, 2009]. However, the 18 year proxy time series shows that conformity of response in all three passages is not always the case (Figure 6). There are occasional periods when there is similarity in the variability between any two of the outflow passages, such as upper layer Lombok and Ombai transport from 1995 through 1999, upper layer Timor and Lombok transport from 2004 through 2010, and lower layer Timor and Ombai transport from 1996 through 1999 (Figure 6). Then there are other periods when there is very little conformity in transport variability between any of the passages. The relationship of this transport variability to ENSO and IOD phases will be discussed in section 4.3.

There is a considerable change in the characteristics of the transport through Lombok Strait from 2006 through 2010 (Figure 6a). In particular, stronger episodic transport into the Indian Ocean occurred in 2006, 2008, and 2009 after a prolonged period of weak variability in the earlier part of the decade. This latter period also directly coincides with a dramatic change in the velocity upstream in Makassar Strait, when the core of subsurface velocity maximum shoaled from ~ 140 m to ~ 70 m depth and also substantially strengthened, resulting in a 47% increase in transport [Gordon *et al.*, 2012]. After a drawn-out period of mild El Niño like conditions in the early decade of the 21st century, Gordon *et al.* [2012] attributed the change in the vertical profile as a response to the return of stronger contrasting La Niña and El Niña transitions in 2006. It is likely that the change in the nature of the transport downstream through Lombok Strait is due to the same phenomena.

In the mid-1990s, the tropical Pacific easterlies strengthened and this intensification is thought responsible for the rising sea level trend in the western tropical Pacific observed in both the AVISO sea level and

SEM in Lombok (August–September) and Ombai (September–October). The semiannual signal is not quite as enhanced in the upper layer of the predicted Lombok and Ombai Strait annual cycle (Figure 5a). Transport through the deeper Ombai Strait is minimum during the monsoon transition periods of April and September when the downwelling Wyrki jets reverse the transport at depth (Figure 5b). Although the phasing of the deep semiannual signal is quite good, differences in magnitude of ~ 1 – 2 Sv occur between the observed and proxy transports during these semiannual peaks (Figure 5b). The predicted and INSTANT transport of the lower layer of Timor Strait agree well, and the proxy time series depicts the strong semiannual signal that shows different phasing with Ombai Strait (Figure 5b). The full depth transports (from the addition of the upper and lower layer transports) show remarkably good agreement with the observed total transport (Figure 5c).

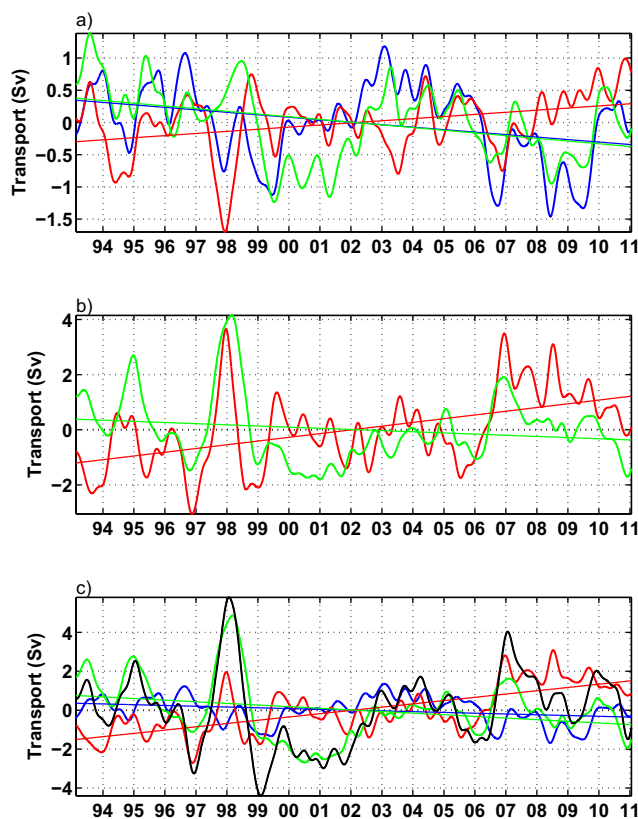


Figure 6. Time series of predicted transports in Lombok Strait (blue), Ombai Strait (red), and Timor Passage (green) over the depth range (a) 0–150 m; (b) 150 m to sill depth; and (c) full depth. Total full depth transport summed over all three passages is shown in black in Figure 6c.

sequently, there is only a small decrease of 0.5 Sv in total ITF transport through all three passages over the 18 year period.

4.3. Response to ENSO and IOD Phase

As a first step toward teasing out the potential partitioning of the transport through each outflow strait in response to the phase of ENSO and the IOD, composites of the transport time series were formed according to whether the period consisted of either solely an El Niño or La Niña event, or of a coincident El Niño (La Niña) event with a positive (negative) IOD phase (Table 1). In the 18 year time series, there were no coincident El Niño events with negative IOD events, and only one year had a coinciding La Niña and IOD positive event (Table 1), so given the relatively small sample size, we will not discuss the transport response of the ITF during these concurrent phases. Both IOD and ENSO phases typically begin in the boreal spring and peak (ENSO) or terminate (IOD) in the boreal winter. Once ENSO peaks, the processes that facilitate the event's demise the following spring tend to kick in [McGregor et al., 2013]. Hence, in order not to introduce any alias due to these competing terminating processes, the composites will be constructed to span from July through December. The long-term trend of each time series (e.g., Figure 6) was removed before forming the composites.

In the upper 150 m, transport through both Lombok and Timor Passage is significantly reduced during El Niño events (Figure 7a). However, in Ombai Strait, the reduction in the upper layer is not significant (red bars in Figure 7a show the standard error of the mean passes through zero), while in the deeper layer below 150 m the transport is 0.5 Sv stronger than normal during El Niño events (Figure 7b). The competing impact of the transport changes in both the upper and lower layer cancel out any anomalous transport changes in the total transport (Figure 7c). Subsequently, the expected response of a reduced total ITF to the relaxation in the Pacific wind field during El Niño events [Wyrski, 1987] occurs only in the upper layer of Lombok and Timor. A time series of the composite suggests this begins in October, around 5 months following the onset

regional tide gauge records [Merrifield, 2011]. Since it is this higher Pacific sea level that is thought to drive the ITF on annual and longer time scales [Wyrski, 1987], we might expect an increased ITF transport over the 20 year period, as suggested by a suite of ocean data assimilation products and ocean models [Lee and McPhaden, 2008; Merrifield et al., 2009; Lee et al., 2010; Merrifield and Maltrud, 2011]. A significantly increased ITF transport of ~ 0.6 Sv over the 18 year time period is observed in both the upper layer of Lombok Strait and Timor Passage (both passages have linear trends of -0.04 ± 0.003 Sv per year), with a similar increase observed in the lower layer of Timor Passage (-0.042 ± 0.003 Sv per year) (Figure 6). However, a decrease in ITF transport in both the upper and lower layers of Ombai Strait of ~ 0.5 Sv (0.03 ± 0.001 Sv per year) and ~ 2.5 Sv (0.135 ± 0.003 Sv per year) also occurs over the 18 year period, respectively. Subse-

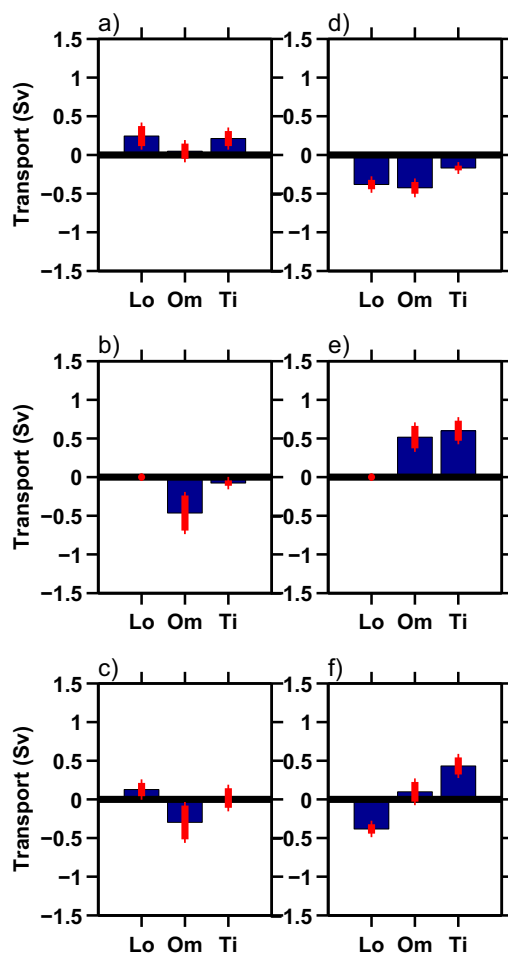


Figure 7. Anomalous transport through Lombok (Lo), Ombai (Om), and Timor (Ti) during (left) solo El Niño events and (right) coincident El Niño and positive IOD events over the (a and d) upper 150 m depth, (b and e) from 150 m to sill depth, and (c and f) full depth. The red lines indicate standard error for each estimate.

There is no significant impact of solo La Niña events on the transport through either Lombok or Ombai Straits. When La Niña events coincide with negative IODs, there is reduced transport in the upper layer of all three straits, but particularly Timor Passage (Figure 8d) and stronger transport at depth through Ombai Strait and weaker transport at depth through Timor Passage (Figure 8e). However, since there are only two years when these events coincide (Table 1), the error bars are large and the results should be treated with caution.

5. Relationship of Transport to Winds and Large-Scale Forcing

The relationship of the ITF transport variability to the remote wind forcing from the Indian and Pacific Oceans during concurrent ENSO and IOD events has received much attention from numerical modelers [e.g., Murtugudde *et al.*, 1998; Feng *et al.*, 2001; England and Huang, 2005; Potemra and Schneider, 2007]. Equatorial boxes of wind stress anomalies in the Indian Ocean and Western Pacific Ocean show that during concurrent ENSO and IOD events (Table 1), the wind stresses are correlated but out of phase (Figure 9)—a modulation of the Walker circulation. This partial anticorrelation between Pacific and Indian equatorial zonal winds can result in a partial cancellation of the wind effect on the ITF transport: the anomalous Indian easterlies and Pacific westerlies both tend to drop dynamic height in the ITF region, and thus the large-scale pressure gradient driving the ITF may not be much affected. However, during these concurrent events the Pacific wind changes are much weaker compared to those in the Indian Ocean, sometimes by as much as 50%, suggesting that the partial cancellation effect may not be the complete story.

of an El Niño event and continues until the following boreal spring (not shown). In contrast, when an El Niño event coincides with a positive IOD event, the transport through all three straits is stronger in the upper 150 m, particularly Lombok and Ombai (Figure 7d), and significantly reduced by ~ 0.5 Sv in the lower layers below 150 m of both Ombai and Timor Passage (Figure 7e). In the upper layer of Lombok and Ombai, the enhanced ITF begins only one month after the onset of the positive IOD/ENSO event in May, reaches a maximum around November and then quickly diminishes in January (not shown). In the lower layer of both Ombai and Timor, the reduced ITF begins around July, is maximum around December and returns to normal the following February. These timings are consistent with positive IOD phases [Saji *et al.*, 1999].

In the case of solo La Niña events, there is significantly more transport through Timor Passage in both the upper 150 m (Figure 8a) and below 150 m (Figure 8b), with a total anomalously strong transport of ~ 1.0 Sv (Figure 8c).

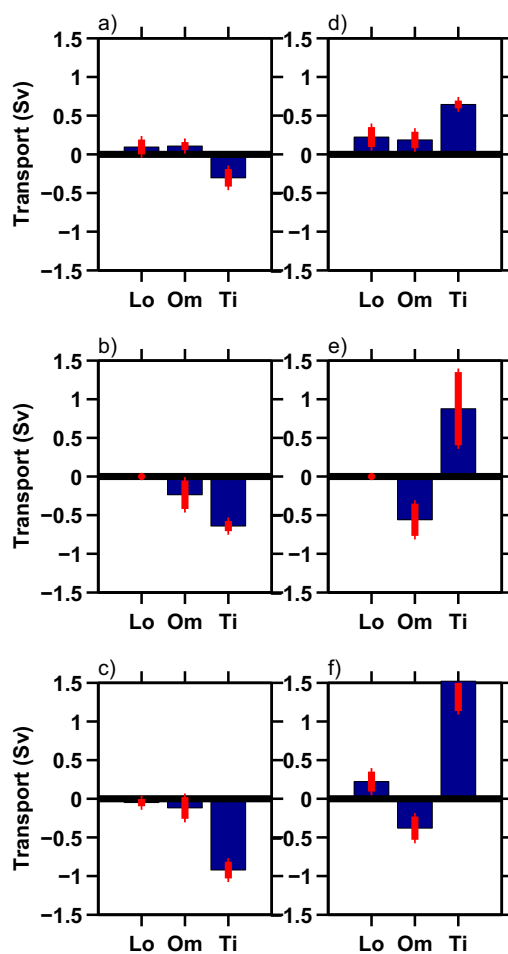


Figure 8. Anomalous transport through Lombok (Lo), Ombai (Om), and Timor(Ti) during (left) solo La Niña events and (right) coincident La Niña and negative IOD events over the (a and d) upper 150 m depth, (b and e) from 150 m to sill depth, and (c and f) full depth. The red lines indicate standard error for each estimate.

into Lombok Strait [Clarke and Liu, 1994; Meyers, 1996; Potemra, 2001; Wijffels and Meyers, 2004]. During concurrent El Niño and positive IOD episodes there are significantly stronger easterly winds evident in the eastern equatorial Indian Ocean (Figure 10d). These winds have resulted in the lower sea level evident along the Sumatra and Java coasts (Figure 10c) as a result of upwelling Kelvin waves [e.g., Sprintall *et al.*, 2009] and/or due to offshore Ekman transport [Potemra and Schneider, 2007]. In either event, both phenomena would act to enhance the upper layer transport (e.g., Figure 7d). The weaker transport at depth is likely in response to the intermittent but strong downwelling Kelvin waves, such as occurred during the 2006 co-IOD and ENSO episodes [Horii *et al.*, 2008].

In contrast to solo El Niño events, during solo La Niña events there is only marginal impact on the SLA patterns across the tropical Pacific (Figure 11a) in response to the stronger easterlies during this ENSO phase (Figure 11b). Interestingly, there is slightly higher SLA in the latitude bands around 5–10° (Figure 11a) that could possibly be related to off-equatorial Rossby waves driving significantly stronger transport through Timor Passage during these events (Figures 8a and 8b) [e.g., McClean *et al.*, 2005]. During concurrent La Niña and negative IOD events, there is a strong SSH response in both the Pacific and Indian Ocean basins (Figure 11c) compared to solo La Niña events (Figure 11a), with higher SLA evident throughout the Indonesian archipelago. In the tropical Indian Ocean, the anomalous westerly winds force downwelling Kelvin waves that reverse the transport in the upper layer of the outflow passages (Figure 8d).

Examination of the spatial patterns of SLA and zonal wind stress anomalies during ENSO and IOD events in boreal fall (September through November) better illustrates the large-scale variability and here we suggest how this variability impacts on the observed patterns of ITF transport. During solo El Niño events, as expected the SLA pattern is dominated by an eastward positive sea level gradient in the tropical Pacific (Figure 10a), while the zonal winds are out of phase but of near equal anomalous strength in the Pacific and Indian Oceans leading to divergence and suppressed precipitation over the Indonesian archipelago [Meyers *et al.*, 2007]. During these solo El Niño periods, there is reduced upper layer flow in both Lombok and Timor Straits (Figure 7a). This expected response of the ITF transport to El Niño conditions is likely driven by the low-frequency Pacific wind stress curl variability generating Rossby waves that induce coastal-trapped waves propagating poleward along the coast of Irian Jaya and North-west Australia through Timor Passage, as well as westward through the Banda Sea and

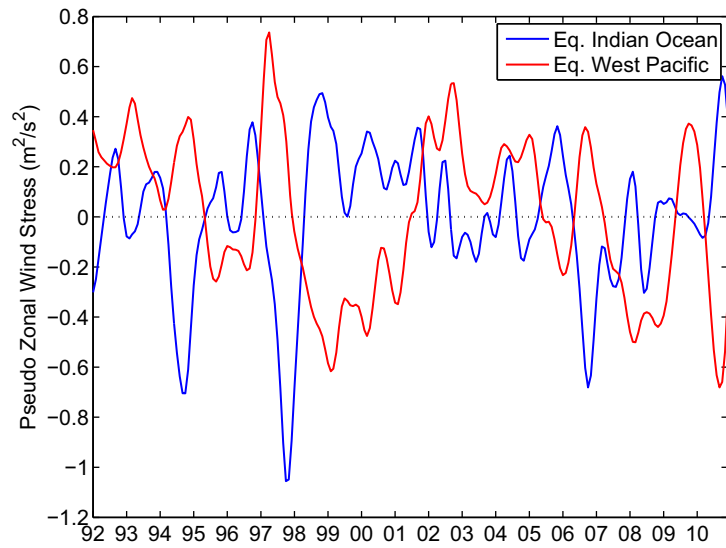


Figure 9. Equatorial pseudo zonal wind stress ($m^2 s^{-2}$) in the western Pacific (red) and Indian Ocean (blue).

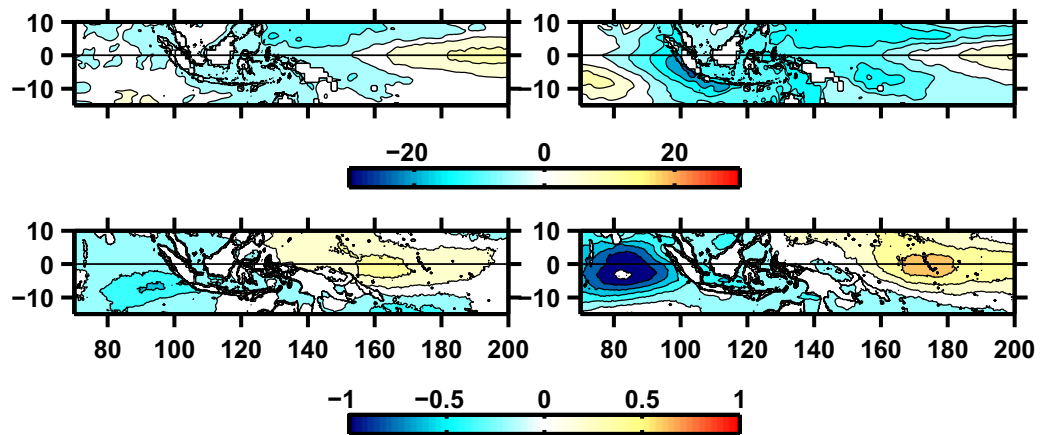


Figure 10. (top) Sea level (cm) and (bottom) pseudo zonal wind ($m^2 s^{-2}$) stress anomalies in September–November during (left) El Niño events and (right) concurrent El Niño and positive IOD events.

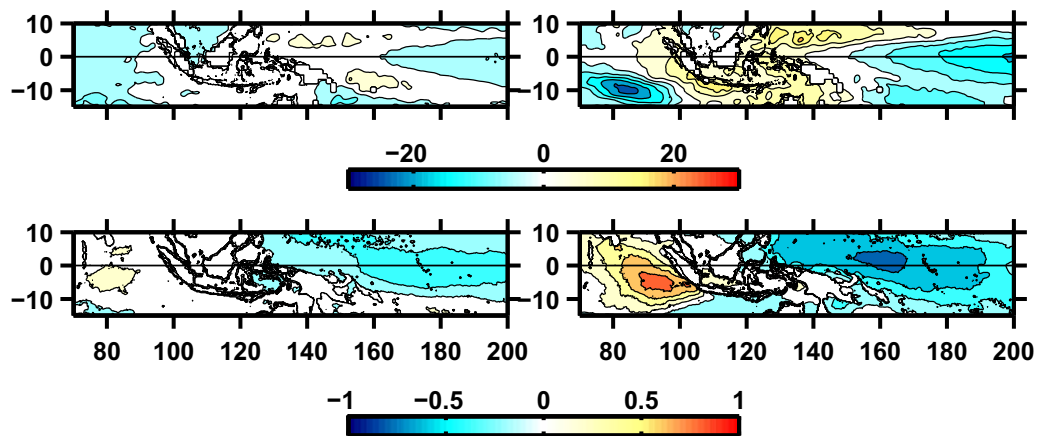


Figure 11. (top) Sea level (cm) and (bottom) pseudo zonal wind stress ($m^2 s^{-2}$) anomalies in September–November during (left) La Niña events and (right) concurrent La Niña and negative IOD events.

6. Conclusions

An 18 year proxy ITF transport time series was developed using a linear, lagged partial regression relationship from a 3 year observed transport time series through each of the three main outflow passages—Lombok, Ombai and Timor—and the regional SLA variability. Our approach exploited the relationship between the ITF transport and the large-scale Indo-Pacific sea level gradient that Wyrski [1987] suggested as being wind-driven, although Andersson and Stigebrandt [2005] suggest the gradient may be a result of stratification differences. The proxy time series was used to examine long-term changes in the ITF transport, how the partitioning of the total ITF transport through each of the major outflow passage varies according to the phase of the IOD or ENSO, and how these changes vary in response to local and large-scale remote wind forcing.

Overall, only Timor Passage consistently behaved as expected under ENSO conditions: weaker transport was observed in the upper layer during composite El Niño events, and stronger transport was observed in both upper and lower layer transport during composite La Niña events. This Timor-Northwest Australian shelf pathway for low-frequency Pacific forcing has been identified in the past in relationship to ENSO variability [e.g., Meyers, 1996; Wijffels and Meyers, 2004; McClean *et al.*, 2005; England and Huang, 2005], and more recently in relationship to the transmission of decadal time-scale thermocline and sea level anomalies [Schwarzkopf and Böning, 2011]. In addition, trends showed a significant increase in transport through Timor Passage over the past 18 years, most likely in response to the increase in sea level and strengthening trade winds in the western Pacific that have been recorded since the early 1990s [Lee and McPhaden, 2008; Merrifield, 2011; Merrifield and Maltrud, 2011; Feng *et al.*, 2011]. However, on decadal and longer time scales, numerous studies have suggested that there is likely to be a weakening of the Walker Circulation in response to a warming climate [Vecchi *et al.*, 2006; Held and Soden, 2006; Tokinaga *et al.*, 2012] and that this should act to diminish the size and strength of the ITF [Wainwright *et al.*, 2008; Sen Gupta *et al.*, 2012], resulting in a shoaling thermocline with cooling on the corresponding isopycnal surfaces in the Indian Ocean [Alory *et al.*, 2007; Wainwright *et al.*, 2008]. Our results suggest that this large-scale Pacific driven variability will most strongly impact the outflow through Timor Passage that lies along the main transmission pathway from the Pacific.

In Lombok Strait, similar to Timor Passage the upper layer transport decreased in response to El Niño events, however there was no transport response at all in Lombok Strait during La Niña events. There was also a significant increase in transport in Lombok Strait over the 18 year transport record, and in particular, substantial transport increases were evident during the 2006–2010 period. As noted above, this latter variability is most likely related to upstream changes in the nature of the flow through Makassar Strait [Gordon *et al.*, 2012]. Interestingly Gordon *et al.* [2012] attributed the change in the Makassar Strait profile as being ENSO induced: during El Niño episodes there is enhanced flow of freshwater from the Sulu Sea into the surface layer of the Sulawesi Sea that acts to block the inflow of warm Pacific surface water resulting in a deeper, cooler velocity core into Makassar Strait, while during La Niña episodes there is little input from the Sulu Sea leading to an increase and shoaling of the warm Pacific water into Makassar Strait. Such a direct link to ENSO variability is not as clear in the Lombok Strait transport, especially in relation to La Niña events, although this may be because of the stronger influence of IOD episodes on Lombok Strait variability, as discussed further below. However, it is clear that the increase in Lombok transport into the Indian Ocean occurred in tandem with the enhanced inflow via Makassar Strait, and furthermore it is evident that much of this additional inflow exited via Lombok Strait as opposed to via Ombai Strait, which was characterized by a decrease in transport over this same period.

It is worth explicitly pointing out that we also examined our ITF time series for any correlation or coherence with central Pacific or so-called Modoki El Niño [Ashok *et al.*, 2007]. However, there was a near-zero relationship between the ITF transport through any of the outflow passages and a Modoki El Niño index. Actually, this is not so surprising since warm events that peak in the central/western Pacific typically show negligible thermocline depth anomalies, so that the recharge/discharge processes often associated with ENSO events are weak or absent [Capotondi, 2013]. Since these processes are intimately linked to the large-scale sea level gradient that drives the ITF on interannual time scales, this gels with the lack of response in ITF transport variability to Modoki El Niño conditions.

Even with an 18 year time series, we were unable to cleanly separate out the impact of ENSO from IOD variability on the transport through the exit passages. This is primarily because of the six El Niño events that

occurred over the 18 years, three co-occurred with positive IOD events, and of the six La Niña events only two co-occurred with negative IOD events so limiting their statistical dependability. In addition, the different responses are also likely dependent on the strength of the events. For example, stronger El Niños are thought to initiate positive IOD events, while solo El Niños tend to be weaker [Kug and Kang, 2006]. Nonetheless, those composites composed of concurrent El Niño and positive IOD episodes consistently showed contradictory results from those composites constructed for purely El Niño episodes. This is particularly evident in Lombok and Ombai Straits, but there is also a significantly strong response at depth in Timor Strait. This suggests that Indian Ocean dynamics likely win out over Pacific Ocean dynamics in gating the collective transport through the outflow passages during concurrent ENSO and IOD events.

Our study concludes with an important caveat: full-depth velocity and property measurements are still needed in the outflow passages to verify these proxy transports and to obtain the climatically meaningful direct estimates of the heat and freshwater transport profiles into the Indian Ocean. Such measurements are presently underway in Ombai Strait and Timor Passage (S. Wijffels, personal communication, 2013). Still, with such a relatively short record it will likely remain difficult to tease out the competing remote influences from ENSO and the IOD on the ITF transport variability. Clearly, a longer proxy time series will serve as an important building block for better assessing long-term climate trends such as the changing Walker Circulation, that are likely to result in a varying ITF that impacts the Indo-Pacific region and beyond.

Acknowledgments

This work was supported by NASA grant NNX13AO38G. The study was initiated during an internship by Ms. Adèle Révelard at Scripps Institution of Oceanography in 2012 supported by Ecole Normale Supérieure, Paris. We are gratefully indebted to Robert Molcard for providing the 1996 mooring data from Ombai Strait. The ENSO index was downloaded from http://www.cpc.ncep.noaa.gov/products/analysis_monitoring/ensostuff/ensoyears.shtml and the IOD index from <http://www.jamstec.go.jp/frgcr/research/d1/iod/HTML/Dipole%20Mode%20Index.html>. The altimeter products were produced by Ssalto/Duacs and distributed by Aviso, with support from CNES (<http://www.aviso.oceanobs.com/duacs/>). The CCMP wind data were obtained from the Physical Oceanography Distributed Active Archive Center (PO.DAAC) at the NASA Jet Propulsion Laboratory, Pasadena, CA (<http://podaac.jpl.nasa.gov>).

References

- Alory, G., S. E. Wijffels, and G. Meyers (2007), Observed temperature trends in the Indian Ocean over 1960–1999 and associated mechanisms, *Geophys. Res. Lett.*, *34*, L02606, doi:10.1029/2006GL028044.
- Andersson, H.C., and A. Stigebrandt (2005), Regulation of the Indonesian throughflow by baroclinic draining of the North Australian Basin, *Deep-Sea Res. I*, *52*, 2214–2233, doi: 10.1016/j.dsr.2005.06.014.
- Ashok, K., S. K. Behera, S. A. Rao, H. Weng, and T. Yamagata (2007), El Niño Modoki and its possible teleconnection, *J. Geophys. Res.*, *112*, C11007, doi:10.1029/2006JC003798.
- Atlas, R., R. N. Hoffman, J. Ardzizzone, S. M. Leidner, J. C. Jusem, D. K. Smith, and D. Gombos (2011), A cross-calibrated, multiplatform ocean surface wind velocity product for meteorological and oceanographic applications, *Bull. Am. Meteorol. Soc.*, *92*, 157–174, doi:10.1175/2010BAMS2946.1.
- Atmadipoera, A., R. Molcard, G. Madec, S. Wijffels, J. Sprintall, A. Koch-Larrouy, I. Jaya, and A. Supagat (2009), Characteristics and variability of the Indonesian Throughflow Water at the Outflow Straits, *Deep Sea Res., Part I*, *56*(11), 1942–1954, doi:10.1016/j.dsr.2009.06.004.
- Capotondi, A. (2013), ENSO diversity in the NCAR CCSM4 climate model, *J. Geophys. Res.*, *118*, 4755–4770, doi:10.1002/jgrc.20335.
- Clarke, A.J., and X. Liu (1993), Observations and dynamics of semiannual and annual sea levels near the eastern equatorial Indian Ocean boundary, *J. Phys. Oceanogr.*, *23*, 386–399.
- Clarke, A. J., and X. Liu (1994), Interannual sea level in the northern and eastern Indian Ocean, *J. Phys. Oceanogr.*, *24*, 1224–1235.
- Drushka, K., J. Sprintall, and S. T. Gille (2010), Vertical structure of Kelvin waves in the Indonesian Throughflow exit passages, *J. Phys. Oceanogr.*, *40*, 1965–1987.
- Efron, B., and G. Gong (1983), A leisurely look at the bootstrap, the jackknife, and cross-validation, *Am. Stat.*, *37*(1), 36–48.
- England, M. H., and F. Huang (2005), On the interannual variability of the Indonesian Throughflow and its linkage with ENSO, *J. Clim.*, *18*, 1435–1444.
- Feng, M., G. Meyers, and S. E. Wijffels (2001), Interannual upper ocean variability in the tropical Indian Ocean, *Geophys. Res. Lett.*, *28*, 4151–4154.
- Feng, M., C. W. Böning, A. Biastoch, E. Behrens, E. Weller, and Y. Masumoto (2011), The reversal of the multi-decadal trends of the equatorial Pacific easterly winds, and the Indonesian Throughflow and Leeuwin Current transports, *Geophys. Res. Lett.*, *38*, L11604, doi:10.1029/2011GL047291.
- Ferrari, R., C. Provost, A. Renault, N. Sennéchal, N. Barré, Y.-H. Park, and J. H. Lee (2012), Circulation in Drake Passage revisited using new current time series and satellite altimetry: 1. The Yaghan Basin, *J. Geophys. Res.*, *117*, C12024, doi:10.1029/2012JC008264.
- Godfrey, J. S. (1996), The effect of the Indonesian Throughflow on ocean circulation and heat exchange with the atmosphere: A review, *J. Geophys. Res.*, *101*, 12,217–12,237.
- Gordon, A. L., R. D. Susanto, and A. Ffield (1999), Throughflow within Makassar Strait, *Geophys. Res. Lett.*, *26*, 3325–3328.
- Gordon, A. L., R. D. Susanto, A. Ffield, B. A. Huber, W. Pranowo, and S. Wirasantosa (2008), Makassar Strait Throughflow, 2004 to 2006, *Geophys. Res. Lett.*, *35*, L24605, doi:10.1029/2008GL036372.
- Gordon, A. L., J. Sprintall, H. M. van Aken, R. D. Susanto, S. E. Wijffels, R. Molcard, A. Ffield, W. Pranowo, and S. Wirasantosa (2010), The Indonesian Throughflow during 2004–2006 as observed by the INSTANT program, *Dyn. Atmos. Oceans*, *50*, 115–128.
- Gordon, A. L., B. A. Huber, E. J. Metzger, R. D. Susanto, H. E. Hurlburt, and T. R. Adi (2012), South China Sea Throughflow Impact on the Indonesian Throughflow, *Geophys. Res. Lett.*, *39*, L11602, doi:10.1029/2012GL052021.
- Held, I. M., and B. J. Soden (2006), Robust responses of the hydrological cycle to global warming, *J. Clim.*, *19*, 5686–5699, doi:10.1175/JCLI3990.1.
- Horii, T., H. Hase, I. Ueki, and Y. Masumoto (2008), Oceanic precondition and evolution of the 2006 Indian Ocean dipole, *Geophys. Res. Lett.*, *35*, L03607, doi:10.1029/2007GL032464.
- Imawaki, S. H. Uchida, H. Ichikawa, M. Fukasawa, S. Umatani, and the ASUKA group (2001), Satellite monitoring the Kuroshio transport south of Japan, *Geophys. Res. Lett.*, *28*, 17–20, doi:10.1029/2000GL011796.
- Kug, J.-S., and I.-S. Kang (2006), Interactive feedback between ENSO and the Indian Ocean, *J. Clim.*, *19*, 1784–1801.
- Lee, T., and M. J. McPhaden (2008), Decadal phase changes in large-scale sea level and winds in the Indo-Pacific region at the end of the 20th century, *Geophys. Res. Lett.*, *35*, L01605, doi:10.1029/2007GL032419.

- Lee, T., I. Fukumori, D. Menemenlis, Z. Xing, and L. L. Fu (2002), Effects of the Indonesian Throughflow on the Pacific and Indian Oceans, *J. Phys. Oceanogr.*, *32*, 1404–1429.
- Lee, T., T. Awaji, M. Balmaseda, et al. (2010), Consistency and fidelity of Indonesian-throughflow total volume transport estimated by 14 ocean data assimilation products, *Dyn. Atmos. Oceans*, *50*(2), 201–223, doi:10.1016/j.dynatmoce.2009.12.004.
- Masumoto, Y., and T. Yamagata (1996), Seasonal variations of the Indonesian Throughflow in a general circulation model, *J. Geophys. Res.*, *101*, 12,287–12,293.
- Masumoto, Y., and G. Meyers (1998), Forced Rossby waves in the southern tropical Indian Ocean, *J. Geophys. Res.*, *103*, 27,589–27,602.
- McClean, J. L., D. P. Ivanova, and J. Sprintall (2005), Remote origins of interannual variability in the Indonesian Throughflow region from data and a global parallel ocean program simulation, *J. Geophys. Res.*, *110*, C10013, doi:10.1029/2004JC002477.
- McGregor, S., N. Ramesh, P. Spence, M. H. England, M. J. McPhaden, and A. Santoso (2013), Meridional movement of wind anomalies during ENSO events and their role in event termination, *Geophys. Res. Lett.*, *40*, 1–6, doi:10.1002/grl.50136.
- Merrifield, M. A. (2011), A shift in western tropical Pacific sea level trends during the 1990s, *J. Clim.*, *24*, 4126–4138, doi:10.1175/2011JCLI3932.1.
- Merrifield, M. A., and M. Maltrud (2011), Regional sea level trends due to Pacific wind intensification, *Geophys. Res. Lett.*, *38*, L21605, doi:10.1029/2011GL049576.
- Merrifield, M. A., S. T. Merrifield, and G. T. Mitchum (2009), An anomalous recent acceleration of global sea level rise, *J. Clim.*, *22*, 5772–5781, doi:10.1175/2009JCLI2985.1.
- Meyers, G. (1996), Variation of Indonesian throughflow and the El Niño–Southern Oscillation, *J. Geophys. Res.*, *101*, 12,255–12,263.
- Meyers, G., P. McIntosh, L. Pigot, and M. Pook (2007), The Years of El Niño, La Niña, and interactions with the tropical Indian Ocean, *J. Clim.*, *20*, 2872–2880, doi:10.1175/JCLI4152.1.
- Molcard, R. M., M. Fieux, and F. Syamsudin (2001), The throughflow within Ombai Strait, *Deep Sea Res., Part I*, *48*, 1237–1253.
- Murtugudde, R., A. J. Busalacchi, and J. Beauchamp (1998), Seasonal to interannual effects of the Indonesian Throughflow on the tropical Indian Ocean basin, *J. Geophys. Res.*, *103*, 21,425–21,441.
- Nicholls, N. (1989), Sea surface temperature and Australian winter rainfall, *J. Clim.*, *2*, 965–973.
- Potemra, J. T. (2001), The potential role of equatorial Pacific winds on southern tropical Indian Ocean Rossby waves, *J. Geophys. Res.*, *106*, 2407–2422.
- Potemra, J. T. (2005), Indonesian Throughflow transport variability estimated from satellite altimetry, *Oceanography*, *18*(4), 98–107.
- Potemra, J. T., and N. Schneider (2007), Interannual variations of the Indonesian Throughflow, *J. Geophys. Res.*, *112*, C05035, doi:10.1029/2006JC003808.
- Potemra, J. T., R. Lukas, and G. Mitchum (1997), Large-scale estimation of transport from the Pacific to the Indian Ocean, *J. Geophys. Res.*, *102*, 27,795–27,812.
- Potemra, J. T., S. L. Hautala, and J. Sprintall (2003), Vertical structure of the Indonesian Throughflow, *Deep Sea Res., Part II*, *50*, 2143–2162.
- Saji, N. H., B. N. Goswami, P. N. Vinayachandran, and T. Yamagata (1999), A dipole mode in the tropical Indian Ocean, *Nature*, *401*, 360–363.
- Schneider, N. (1998), The Indonesian throughflow and the global climate system, *J. Clim.*, *11*, 676–689.
- Schwarzkopf, F. U., and C. W. Böning (2011), Contribution of Pacific wind stress to multi-decadal variations in upper-ocean heat content and sea level in the tropical south Indian Ocean, *Geophys. Res. Lett.*, *38*, L12602, doi:10.1029/2011GL047651.
- Sen Gupta, A., A. Ganachaud, S. McGregor, J. N. Brown, and L. Muir (2012), Drivers of the projected changes to the Pacific Ocean equatorial circulation, *Geophys. Res. Lett.*, *39*, L09605, doi:10.1029/2012GL051447.
- Song, Q., G. A. Vecchi, and A. J. Rosati (2007), The role of the Indonesian Throughflow in the Indo–Pacific climate variability in the GFDL coupled climate model, *J. Clim.*, *20*, 2434–2451, doi:10.1175/JCLI4133.1.
- Sprintall, J., A. L. Gordon, R. Murtugudde, and R. D. Susanto (2000), A semiannual Indian Ocean forced Kelvin wave observed in the Indonesian seas in May 1997, *J. Geophys. Res.*, *105*(C7), 17,217–17,230, doi:10.1029/2000JC900065.
- Sprintall, J., S. Wijffels, A. L. Gordon, A. Ffield, R. Molcard, R. D. Susanto, I. Soesilo, J. Sopaheluwakan, Y. Surachman, and H. M. van Aken (2004), INSTANT: A new international array to measure the Indonesian Throughflow, *EOS Trans. AGU*, *85*(39), 369–376.
- Sprintall, J., S. Wijffels, R. Molcard, and I. Jaya (2009), Direct estimates of the Indonesian Throughflow entering the Indian Ocean, *J. Geophys. Res.*, *114*, C07001, doi:10.1029/2008JC005257.
- Sprintall, J., S. E. Wijffels, R. Molcard, and I. Jaya (2010), Direct evidence of the South Java Current System in Ombai Strait, *Dyn. Atmos. Oceans*, *50*(2), 140–156, doi:10.1016/j.dynatmoce.2010.02.006.
- Tokinaga, H., S.-P. Xie, A. Timmermann, S. McGregor, T. Ogata, H. Kubota, and Y. M. Okumura (2012), Regional patterns of tropical Indo-Pacific Climate change: Evidence of the Walker Circulation weakening, *J. Clim.*, *25*, doi:10.1175/JCLI-D-11-00263.1.
- van Sebille, E., L. M. Beal, and A. Biastoch (2010), Sea surface slope as a proxy for Agulhas Current strength, *Geophys. Res. Lett.*, *37*, L09610, doi:10.1029/2010GL042847.
- Vecchi, G. A., B. J. Soden, A. T. Wittenberg, I. M. Held, A. Leetma, and M. J. Harrison (2006), Weakening of tropical Pacific atmospheric circulation due to anthropogenic forcing, *Nature*, *441*, 73–76, doi:10.1038/nature04744.
- Vinayachandran, P. N., J. Kurian, and C. P. Neema (2007), Indian Ocean response to anomalous conditions in 2006, *Geophys. Res. Lett.*, *34*, L15602, doi:10.1029/2007GL030194.
- Vranes, K., A. L. Gordon, and A. Ffield (2002), The heat transport of the Indonesian throughflow and implications for the Indian Ocean heat budget, *Deep Sea Res., Part II*, *49*, 1391–1410.
- Wainwright, L., G. Meyers, S. Wijffels, and L. Pigot (2008), Change in the Indonesian Throughflow with the climatic shift of 1976/77, *J. Geophys. Res.*, *35*, L03604, doi:10.1029/2007GL031911.
- Wijffels, S., and G. Meyers (2004), An intersection of oceanic wave guides: Variability in the Indonesian Throughflow region, *J. Phys. Oceanogr.*, *34*, 1232–1253.
- Wyrtki, K. (1987), Indonesian Throughflow and the associated pressure gradient, *J. Geophys. Res.*, *92*, 12,941–12,946.